Snapshots of Conformational Changes Shed Light into the NtrX Receiver Domain Signal Transduction Mechanism

Ignacio Fernández[1], Lisandro H. Otero[1,2], Sebastián Klinke[1,2], Mariela del Carmen Carrica[1] and Fernando A. Goldbaum[1,2]

1 - Fundación Instituto Leloir, *IIBBA-CONICET, Av. Patricias Argentinas 435, C1405BWE Buenos Aires, Argentina*
2 - Plataforma Argentina de Biología Estructural y Metabolómica PLABEM, *Av. Patricias Argentinas 435, C1405BWE Buenos Aires, Argentina*

Correspondence to Fernando A. Goldbaum: *fgoldbaum@leloir.org.ar*
http://dx.doi.org/10.1016/j.jmb.2015.06.010
Edited by N. G. Ahn

Abstract

Brucella abortus is an important pathogenic bacterium that has to overcome oxygen deficiency in order to achieve a successful infection. Previously, we proved that a two-component system formed by the histidine kinase NtrY and the response regulator NtrX is essential to achieve an adaptive response to low oxygen tension conditions. Even though the relevance of this signaling pathway has already been demonstrated in other microorganisms, its molecular activation mechanism has not yet been described in detail. In this article, we report the first crystal structures from different conformations of the NtrX receiver domain from *B. abortus*, and we propose a sequence of events to explain the structural rearrangements along the activation process. The analysis of the structures obtained in the presence of the phosphoryl group analog beryllofluoride led us to postulate that changes in the interface formed by the α4 helix and the β5 strand are important for the activation, producing a reorientation of the α5 helix. Also, a biochemical characterization of the NtrX receiver domain enzymatic activities was performed, describing its autophosphorylation and autodephosphorylation kinetics. Finally, the role of H85, an important residue, was addressed by site-directed mutagenesis. Overall, these results provide significant structural basis for understanding the response regulator activation in this bacterial two-component system.

Introduction

Bacteria use two-component signal transduction pathways to sense environmental stimuli and generate adaptive responses [1]. These systems are formed by two conserved components, a histidine kinase (HK) and a response regulator (RR). The HK is typically the input component designed to sense stimuli and correspondingly regulate the signaling pathway. On the other side, the RR is the output of the system, regulated by the HK, and effecting the cellular response. External signals modulate the activity of the HK, which autophosphorylates at a particular histidine residue, creating a high-energy phosphoryl group that is transferred to a conserved aspartate residue of the RR, inducing a conformational change that activates it.

The RR superfamily has a modular architecture and is defined by a conserved regulatory or receiver (REC) domain [2], which participates in catalysis of phosphoryl transfer from the HK to itself and modulates the activity of an effector domain in a phosphorylation-dependent manner. With the use of the same active site, the REC domain has also enzymatic activity to promote its autophosphorylation using high-energy, small-molecule phosphodonors (such as acetyl phosphate, phosphoramidate, carbamyl phosphate, etc.) [3–5]. Despite that the rate of this reaction is typically ~ 100-fold slower than those observed with cognate HKs as donors, most of the *in vitro* analysis of RR phosphorylation has been conducted with small phosphodonors. REC domains are also able to catalyze their autodephosphorylation. Acyl phosphates are inherently unstable,

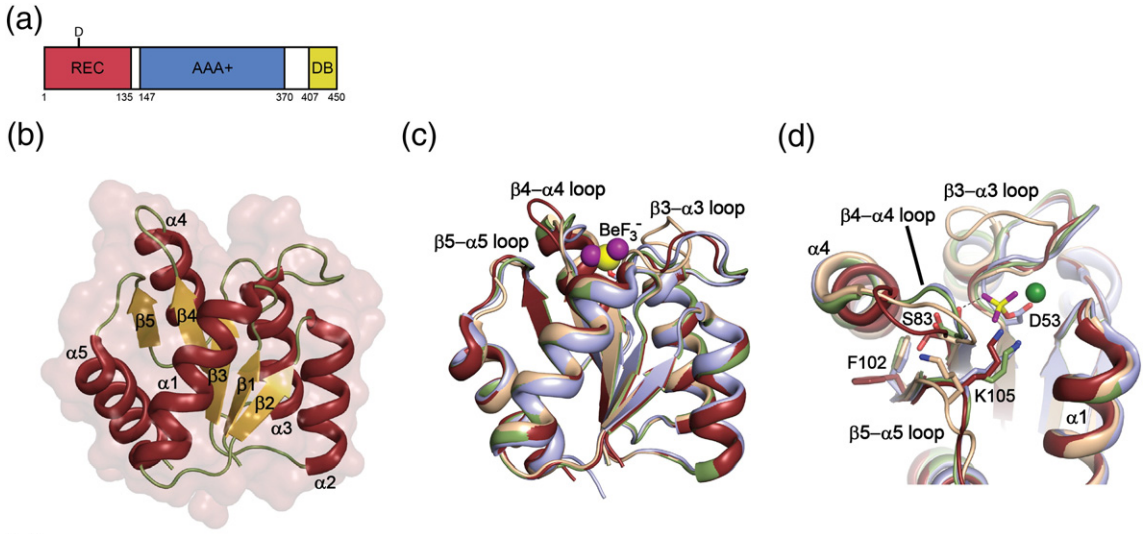

(e)

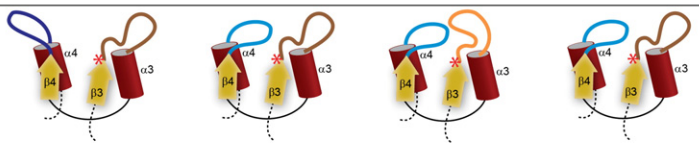

Molecule	A = B	C	D	E = F
BeF_3^-	No	No	No	Yes
Loop β3-α3	Open	Open	Closed	Open
Loop β4-α4	Open	Closed	Closed	Closed
B.S.A. (Å^2)	431	546		600
Conformation	Inactive	Meta-active	Meta-active	Active

Fig. 1. Structural states from NtrX REC domain. (a) NtrX architecture. The REC, AAA+, and DB domains are depicted in red, blue, and yellow, respectively. The phosphorylatable aspartate residue (D53) is highlighted on the REC domain. The numbers indicate each domain boundaries. (b) Cartoon representation of the NtrX REC domain structure in the native state (REC-N) with the secondary structure elements labeled. (c) Structural comparison of molecules A (red), C (green), and D (wheat) from REC-N, along with molecule E (light blue) from REC-A. The position of the key loops β3-α3, β4-α4, and β5-α5 is labeled and the beryllofluoride moiety (BeF_3^-) is represented with yellow and violet spheres. (d) Close-up view of the aligned structures as reported in (c), indicating the position of the residues D53 (bound to BeF_3^-, yellow and violet sticks), S83 (β4 strand), and F102 (β5 strand). The different positions of β3-α3, β4-α4, and β5-α5 loops, as well as α4 helix reorientation, are shown. (e) Schematic representations of the different conformations found in the REC domain crystals. The β3-α3 and β4-α4 loops are drawn in brown and blue, respectively. The open (dark colors) or closed (light colors) state is highlighted. In the schemes, the position of D53 is indicated with a red asterisk. The table also informs whether BeF_3^- is present in the structure, the buried surface area (B.S.A.) between the indicated molecules, and their respective conformational state.

which hinders structural studies of RRs in their phosphorylated active forms. Given this handicap, several *in vitro* approaches have been developed to create stable phosphoryl group analogs, such as beryllofluoride, which forms a tightly bound complex with many RR proteins, mimicking the phosphorylated state [6].

Our laboratory is interested in the signaling pathways involved in the virulence of *Brucella abortus*, an intracellular Gram-negative bacterium that causes abortion and sterility in domestic animals and undulant fever in humans [7]. Given the reported relevance of low oxygen tension during *Brucella* infection [8–10], we are particularly interested in two-component systems that could participate in an adaptive response to such environmental signal [11,12]. In this regard, we described that the NtrY HK is activated upon reduction and is necessary for induction of adaptive pathways to cope with low oxygen availability. We also demonstrated that, after NtrY autophosphorylation, the phosphoryl group is transferred to NtrX, its cognate RR [11]. With the use of genetic approaches, orthologues of the NtrY/X two-component system have been studied in other microorganisms and have been involved in nitrogen fixation and metabolism in *Azorhizobium caulinodans* (where the system was described for the first time) [13]; inhibition of lysosomal fusion in *Ehrlichia chaffeensis* [14];

Table 1. Data collection and refinement statistics

Statistics	REC-N	REC-A
PDB code	4D6X	4D6Y
Data collection		
Synchrotron source	SOLEIL	SOLEIL
Beamline	PROXIMA 1	PROXIMA 1
Number of frames	700	3000
Oscillation step (°)	0.2	0.1
Detector distance (mm)	343.5	244.3
Wavelength (Å)	0.9785	0.9762
Exposure per frame (s)	0.2	0.1
Indexing and scaling		
Cell parameters		
a (Å)	38.67	30.39
b (Å)	110.94	39.34
c (Å)	119.43	52.96
α (°)	90.00	97.30
β (°)	90.00	96.97
γ (°)	90.00	89.97
Space group	$P2_12_12_1$	$P1$
Resolution limit (Å)	2.11	1.70
Number of total reflections	153,925	75,586
Number of unique reflections	30,141	25,833
Average multiplicity [a]	5.1 (5.3)	2.9 (2.8)
$\langle I/\sigma(I)\rangle$	16.6 (2.0)	9.9 (3.4)
R_{meas}	0.046 (0.651)	0.080 (0.420)
Completeness (%)	98.7 (98.1)	97.2 (95.8)
Monomers per asymmetric unit	4	2
Solvent content (%)	37	35
B-factor (Wilson plot, Å^2)	57	22
Refinement		
Resolution range (Å)	40.6–2.11	20.0–1.70
Number of protein atoms	3712	1880
Number of ligand atoms	15	10
Number of water molecules	83	106
R	0.213	0.184
R_{free}	0.219	0.204
RMSD values from ideal values[b]		
Bond lengths (Å)	0.010	0.010
Bond angles (°)	1.1	1.0
B-factor (average, Å^2)	75	28
MolProbity validation[c]		
Clashscore	3.61	4.23
Poor rotamers (%)	8.9	4.5
Ramachandran plot (%)		
Favored	98.5	100.0
Allowed	1.5	—
Disallowed	—	—

[a] Values in parentheses correspond to the highest-resolution shell: REC-N, 2.24–2.11 Å; REC-A, 1.77–1.70 Å.
[b] From Ref. [57].
[c] From Ref. [51].

expression of respiratory enzymes in the oxidase-positive proteobacteria *Neisseria gonorrhoeae* [15]; and succinoglycan production, motility, and symbiotic nodulation in *Sinorhizobium meliloti* [16]. Noteworthy, the *ntrX* gene was reported to be conditionally essential in *Caulobacter crescentus* [17].

NtrX comprises three domains: (1) an N-terminal REC domain (residues 1–135), (2) a central AAA+ domain (residues 147–370), and (3) a C-terminal helix–turn–helix DNA binding domain (residues 407–450) (Fig. 1a). This organization and sequence similarity classifies NtrX among the members of the NtrC subfamily. Many RRs from this group can act as bacterial enhancer binding proteins (bEBPs), that is, transcriptional factors that hexamerize and regulate σ^{54} promoters (e.g., NtrC, NtrC1, NtrC4, DctD, and ZraR) [18]. Sequence analysis shows that NtrX has a major difference with typical NtrC subfamily members: it lacks a GAFTA motif that is considered a bEBP-specific structural element. Some unusual variants of the bEBP subfamily with an absent GAFTA motif have been reported (*Rhodobacter capsulatus* NtrC, HupR) and regulate transcription at σ^{70} promoters [19,20]. Even though it has not been clearly established which family of promoters is regulated by NtrX, the interaction of this RR with the *putA* and *glnA* promoters was reported in *E. chaffeensis*, a microorganism that encodes only σ^{70} and σ^{32} factors [21].

Since no homologue of NtrX has been previously characterized in detail, we decided to study the structural changes in its receiver domain upon phosphorylation in order to gain insight into the activation mechanism of this RR. Here, we report the first crystal structure of the NtrX receiver domain in its nonphosphorylated state and when bound to beryllofluoride. The models indicate that phosphorylation leads to characteristic conformational changes and tightens an interface formed by the α4 helix and the β5 strand, promoting dimerization of the REC domain. Furthermore, it was possible to crystallize the native REC domain in three conformations, one of which resembles the active state despite the absence of a phosphate analog. We also established the importance of the H85 residue in different catalytic activities of the receiver domain. Altogether, our results provide structural and biochemical information that contributes in understanding how phosphorylation at the REC domain is transduced to the other domains of NtrX and represent the first steps to comprehend the molecular activation mechanism of this RR.

Results

Crystal structure of the NtrX REC domain: Overall description

In order to examine the structural changes linked to the inactive and activated states in the NtrX REC domain, we performed crystallization experiments on a construct encompassing residues 1–126, lacking the last 9 amino acids of the predicted α5 helix (residues 109–135). We decided to work with a construct bearing a truncated α5 helix to increase the chances of crystallization since structural evidence noted in other RR domains showed the projection of this helix outside the protein globular fold (HupR, DctD, NtrC1) [22–24].

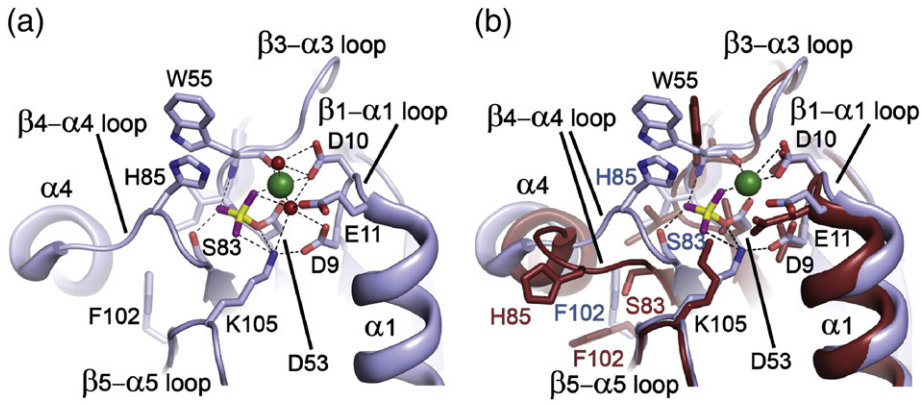

Fig. 2. NtrX REC domain active site. (a) Close-up view of the active site from the REC-A structure (active state). Relevant amino acids are shown in sticks, with carbons in light blue, oxygens in red, and nitrogens in blue. Beryllofluoride is drawn as yellow and violet sticks; magnesium, as green spheres; and water molecules, as red spheres. Polar interactions are depicted as broken lines. The most relevant loops are labeled. (b) Structural contrast between the active sites from the inactive state (red, molecule A from REC-N) and the active state (light blue, molecule E from REC-A). The positions of the crucial residues involved in the activation (S83 and F102) are illustrated.

We solved the three-dimensional structures of this construct in its native state (REC-N) and bound to the phosphorylation-mimic BeF_3^- plus Mg^{2+} (REC-A). REC-N and REC-A crystal structures were solved at medium to high resolutions using the molecular replacement method in the orthorhombic ($P2_12_12_1$) and triclinic ($P1$) space groups, respectively (Fig. 1 and Table 1). The good resolution and the reduced noise in the $2mF_o - DF_c$ electron density maps allowed tracing the complete protein backbone with no chain breaks in both crystal forms. The final refined models show very good stereochemistry, with more than 98.5% of the residues in the favored region of the Ramachandran plot (Table 1).

The NtrX REC domain consists of a five-stranded parallel β-sheet surrounded by five α-helices, forming the canonical $(\beta\alpha)_5$ topology, as found in other structurally solved homologous domains [25] (Fig. 1b). The secondary structure elements are composed of the residues β1 (5–8), α1 (12–24), β2 (29–32), α2 (35–44), β3 (49–52), α3 (63–73), β4 (79–83), α4 (88–96), β5 (101–104), and α5 (109–123). All structural states have a similar global conformation (RMSD < 0.91 Å, calculated between the α-carbons of matched residues), with overall dimensions of 28 Å × 25 Å × 31 Å, and a solvent accessible surface area of approximately 6300 $Å^2$.

The REC-N crystal arrangement bears four molecules in the asymmetric unit (A, B, C, and D; with a highest RMSD value of 0.90 Å between them), with noteworthy differences at the β3-α3 and β5-α5 loops, where A = B = C ≠ D, and at the loop β4-α4 along with the orientation of the helix α4, where A = B ≠ C = D (as described below in detail and in Fig. 1c and e and Fig. S1a). On the other hand, REC-A shows two identical molecules per asymmetric unit (E and F; with a marginal RMSD value of 0.06 Å) (Fig. S1b), which remarkably exhibit a similar conformation with the REC-N molecules C (RMSD = 0.43 Å) and D (RMSD = 0.67 Å, mainly due to differences at the β5-α5 loop) (Fig. 1c).

A PDBeFold server search [26] revealed that the best fits correspond to the RRs from the *Streptococcus pneumoniae* YycF homologue (PDB codes 2A90, 2A9P, and 2A9R; unpublished results), *Escherichia coli* ArcA (PDB codes 1XHF and 1XHE) [27], and *E. coli* PhoB (PDB code 1ZES) [28], among others. The number of aligned residues of REC-N and REC-A with these proteins ranges from 116 to 119, the RMSD ranges from 0.9 to 1.5 Å, and the sequence identity is below 32%.

The native state of the NtrX receiver domain consists of an ensemble of different conformers

The crystal structure of REC-N shows three conformers, with the main differences localized in loops surrounding the phosphorylation site. Specific open–closed states for the β3-α3 and β4-α4 loops are noted, according to their orientation (pointing away from the globular fold or partially covering the active site, respectively) (Fig. 1c and e). The molecules A and B from REC-N display their β3-α3 and β4-α4 loops in open–open states where S83 and F102 (from β4 and β5, respectively) are pointing away of the active site (Fig. 1d), a characteristic conformation of RRs in their inactive state [2,25]. The molecule C from REC-N shows its β3-α3 and β4-α4 loops in open–closed states, and the molecule D has these loops in a closed–closed configuration (Fig. 1c and e). In both cases, the S83 and F102 side chains are turned toward the active site (Fig. 1d). A rearrangement on loop β4-α4 gives rise to a slight twist into strand β4 (clockwise from the N-terminal point of reference) and, consequently, a displacement of helix α4 (see the description below).

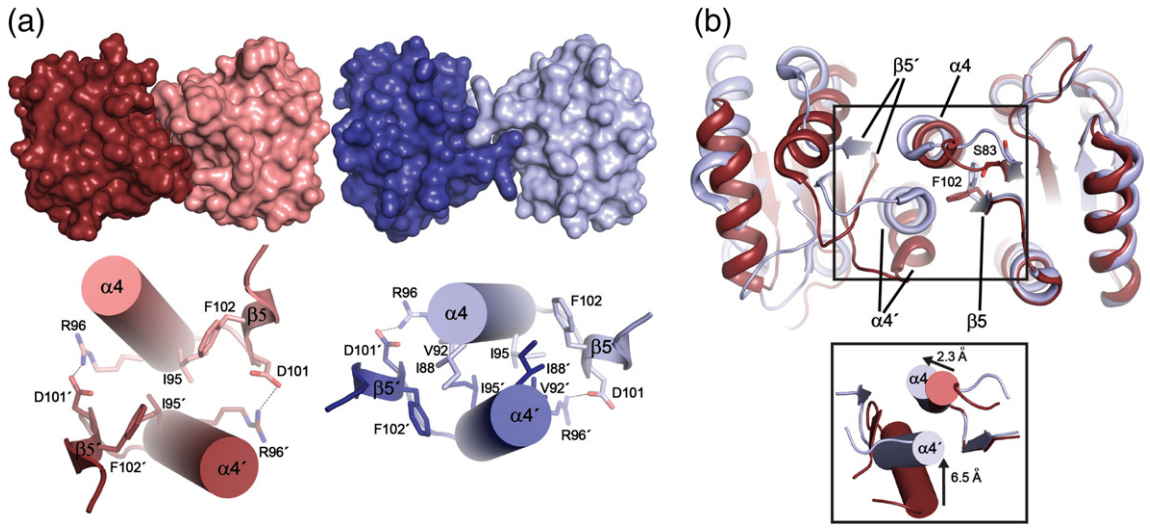

Fig. 3. NtrX REC domain dimer interface. (a) Solvent-accessible surface representation of the dimeric structure of the REC domain in its inactive (red, left panel) and active (light blue, right panel) states. Below these illustrations, the interface formed by α4 and β5 from opposite monomers is depicted, showing polar and hydrophobic contacts. (b) Cartoon representation of the overlay between the dimers A-B from REC-N (red) and E-F from REC-A (light blue). On the active state, α4 helix is displaced tightening the interface (inset). The different conformations of S83 and F102 are also indicated.

Molecules C and D from REC-N remarkably mimic REC-A in terms of the position of the β4-α4 loop, orientation of helix α4, and the inward configuration of S83 and F102 (RMSD = 0.43 Å) (as described below and in Fig. 1c and d). Based on these observations, the molecules A and B from REC-N may correspond to an inactive state, whereas molecules C and D may represent a meta-active conformation (a conformation that resembles the active state despite the absence of a phosphate analog), as has been already reported for CheY and DesR [29,30].

Activation of the receiver domain involves conformational changes at the β4-α4 loop and reorientation of the α4 helix

Analysis of REC-A shows that its active site, formed by conserved residues important for the phosphorylation process, shares a similar architecture with other RR domains [25]. The active site is located at the C-terminal region of the parallel β1, β3, and β4 strands and is partially covered by the loops β1-α1, β3-α3, and β4-α4 (Fig. 2a). Here, a crucial aspartate residue (D53) lying down at the C-terminal end of β3 is found to be responsible for making a nucleophilic attack on the beryllium atom of BeF_3^-. This residue is stabilized through a salt-bridge interaction between K105 and one Mg^{2+} ion. The side chains from residues D9, D10 (β1-α1 loop), W55 (β3-α3 loop), and H85 (β4-α4 loop) encircle the pocket on its top.

The BeF_3^- ligand forms an acyl phosphate analog with the carboxylate of D53 from the active site (Fig. 2a). The three fluoride ions are stabilized by interactions with S83, K105, and main-chain nitrogen atoms of I54, W55, G84, the Mg^{2+} ion, and a water molecule. In addition, a van der Waals contact with the H85 side chain is observed.

When comparing the structures of the inactive and active states (molecules A *versus* E, respectively), significant changes within the active site are noted (Fig. 2b). In the active state, the β4-α4 loop is reoriented toward the β3-α3 loop (around 6.0 Å displacement), which creates a π-stacking interaction between the side chains of W55 and H85 (which are 12.6 Å away from each other in the native state). This is accomplished by the formation of a new interaction between the D53 and K105 side chains (from 4.3 Å in the native state down to 3.3 Å in the active state). This is a consequence of two new salt-bridge interactions between the donor atom N^{ζ} of K105 and the acceptor atom $O^{\delta 1}$ of D9 and a fluorine atom of the BeF_3^- ligand. In addition, the S83 and F102 side chains make a flip, pointing now toward the active site (Figs. 1d and 2b), allowing the interaction between the serine side chain and a fluoride ion, as well as the burying of the phenylalanine. Those changes lead to a movement of the N-terminal region of the α4 helix, which protrudes 2.3 Å outside the protein globular fold (Fig. 2b). It is important to state that loops β3-α3 and β4-α4, despite being exposed on the protein

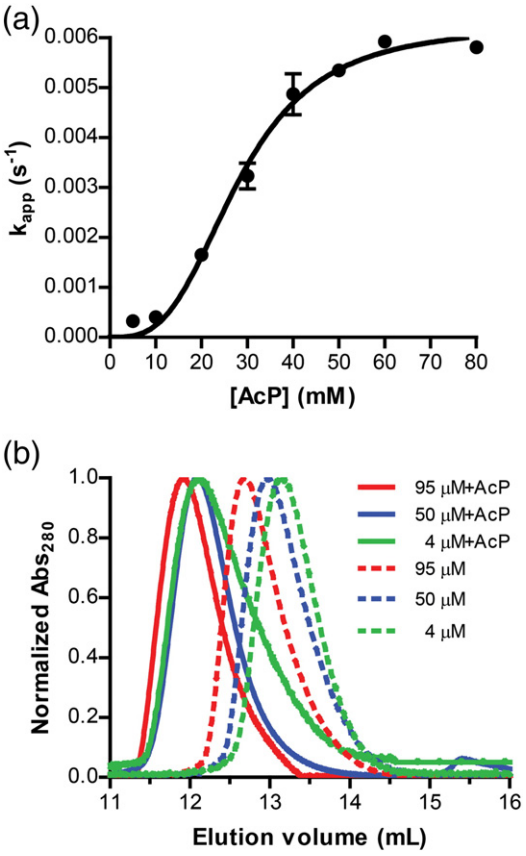

Fig. 4. Biochemical and biophysical assessment of the REC domain quaternary structure. (a) Fluorescence spectroscopy was used to determine the kinetics of NtrX REC domain autophosphorylation with different concentrations of AcP. The rate constant of this reaction performed in triplicate is plotted against the concentration of the phosphodonor with the best-fit sigmoid curve overlaid. (b) SEC profiles of the REC domain in its native state (broken lines) or phosphorylated by previous incubation with AcP (continuous lines). The SLS signal at 90° was also recorded (data not shown) and used, along with the corresponding absorbance at 280 nm, to determine the average MM of the different samples, as expressed in Table 2.

surface, are not involved in major intermolecular interactions.

Active NtrX REC domains exhibit a more extensive interface between monomers

The structural analysis of REC-N reveals a dimeric interface formed by the α4 helix and β5 strand of combined monomers (Fig. 3). This interface can adopt two possible conformations, A-B and C-D. The first one has a buried surface area of 431 $Å^2$ and is observed between molecules from the same asymmetric unit, but the C-D conformer is assembled by chains belonging to adjacent asymmetric units with a buried surface area of 546 $Å^2$ (Fig. S2). In all cases, the two monomers forming the dimer are positioned in the same orientation. The mentioned interface involves mainly a salt-bridge interaction between R96 (N-terminus of the β5 strand) and D101 (C-terminus of the α4 helix) and hydrophobic interactions between I95 from both monomers (Fig. 3a, left). The presence of F102 pointing away from the protein core prevents the assembly of a tighter interface (Fig. 3b). Noteworthy, the C-D dimer interface observed in REC-N shows identical orientation and interactions in comparison with the interface noticed in E-F conformers from REC-A (Fig. S2).

As mentioned before, in REC-A, the helix α4 protrudes outside the protein globular fold, allowing for a more extensive interface in the activated state achieved by additional hydrophobic residues, such as I88, A91, and V92 from this helix (Fig. 3a, right). The salt-bridge interaction between R96 and D101′ is preserved, as well as the hydrophobic contacts between I95 and I95′ (Fig. 3a). In conclusion, despite that the secondary structural elements involved in this interface are the same as those in REC-N, the comparison between the dimer interface from the A-B conformers in REC-N and E-F from REC-A reveals a distorted area, where the rearrangement into helix α4 orientation (Fig. 3b, bottom) causes a greater buried surface area (600 $Å^2$) (Fig. 3a, top).

The NtrX REC domain is under monomer–dimer equilibrium and phosphorylation stabilizes the dimeric form

It has been well established that small-molecule phosphodonors such as acetyl phosphate (AcP) and phosphoramidate represent valuable tools to generate a phosphorylated RR *in vitro* [31]. Moreover, in RRs that bear a tryptophan residue close to the phosphorylatable aspartate (such as W55 in NtrX), the phosphorylation reaction can be studied using fluorescence spectroscopy [31].

A recent report used this approach to propose a model in which the phosphorylation of PhoB is coupled to its dimerization [32] by the formation of a heterodimer between a phosphorylated monomer and a nonphosphorylated monomer. Also, allosteric coupling between dimerization and phosphorylation has been proved for the DesR RR [30]. Then, since autophosphorylation kinetics might provide a functional tool to assess the quaternary structure of the protein, we decided to study the phosphorylation of the NtrX REC domain using AcP. To this end, we incubated different concentrations of the receiver domain with a fixed amount of AcP and Mg^{2+}, and we recorded the changes in fluorescence intensity during a certain period of time to determine the fluorescence quenching of W55. Incubation with AcP leads to a time-dependent fluorescence quenching (Fig. S3), indicating that the reaction with the small phosphodonor occurs and showing

Table 2. Molecular mass (MM) determined by SEC-SLS for the wild type (REC-WT) and mutant (REC-H85A) receiver domains in the nonphosphorylated (−AcP) and phosphorylated (+AcP) states

Protein	Concentration (μM)	MM (kDa) −AcP	MM (kDa) +AcP
REC-WT	500	25.3	ND[a]
	95	21.9	31.0
	50	19.2	30.0
	4	16.8	23.1
REC-H85A	500	22.6	ND[a]
	95	18.9	30.6
			20.4
	50	18.2	29.6
			18.4
	4	16.1	20.2
			15.2

[a] ND, not determined.

that the reaction rate is dependent on the protein concentration. This is consistent with the proposed model for PhoB since higher concentration of the REC domain would favor the formation of the heterodimer whose dimerization constant has been proved to be in the same range as the protein concentration used in our assays [32].

We also performed kinetic experiments with a fixed concentration of the REC domain (10 μM) and increasing amounts of AcP. The fluorescence curves were fitted to a single-exponential decay function and the derived constants were plotted against the concentration of AcP. The results indicate that the autophosphorylation rate varies sigmoidally with the concentration of phosphodonor (Fig. 4a). This apparent positive cooperativity indicated communication between NtrX REC active sites, such that autophosphorylation of one active site led to enhanced autophosphorylation kinetics at other active sites. Altogether, this result, along with the protein concentration dependence, is in agreement with the dimerization of the REC domain associated with its autophosphorylation, as has been described for PhoB [32].

To directly address the oligomeric state of the REC domain in solution, we performed size-exclusion chromatography (SEC) coupled to static light scattering (SLS). The chromatograms show that the elution volume was smaller for increasing concentrations of protein (Fig. 4b and Fig. S4). The molecular mass (MM) estimated in each case (Table 2) depends on the REC domain concentration, being higher when the protein is more concentrated. For example, when injecting the protein at 500 μM into the column, the MM obtained was 25.3 kDa, which is between that expected for a monomer (16 kDa) and that expected for a dimer (32 kDa). This indicates that the REC domain is under a rapid monomer–dimer equilibrium that depends on protein concentration and that the SEC is not able to resolve both populations under these conditions.

When the REC domain was preincubated with AcP, the observed peak shifted to lower elution volumes and the estimated MM agrees better with that expected for the dimeric form (Table 2). This indicates that phosphorylation stabilizes the dimer of the REC domain, which is in agreement with the more extensive interface observed in the crystallographic structures with beryllofluoride. At low protein concentration (4 μM), the MM of the phosphorylated REC was 27 kDa (Table 2) and showed a marked tailing profile. This can be explained by an incomplete phosphorylation since, as we reported before, the phosphorylation reaction depends on protein concentration.

H85 influences the rate of autophosphorylation with AcP and the phosphotransfer efficiency and determines the half-life of the activated REC domain

Previous reports on CheY have demonstrated that its residue E89 (equivalent to H85 in NtrX) modulates the autophosphorylation kinetics, phosphodonor preference [33], and dephosphorylation rate [34]. In the NtrX REC domain structures, H85 is located in the β4-α4 loop (the region with the highest structural plasticity in the transition from the inactive state to the active state) and interacts with W55 in the active conformation (Fig. 2b). Those observations led us to investigate the role of H85, and for this purpose, we decided to perform site-directed mutagenesis experiments in which we replaced this amino acid with alanine (REC-H85A). Using fluorescence spectroscopy, we determined the kinetics of phosphorylation of REC-H85A with AcP. The mutant domain is severely impaired to autophosphorylate, as can be deduced from the markedly reduced rate constants obtained at different AcP concentrations when compared to those obtained for REC-WT (Table 3).

Given that result and taking into consideration that autophosphorylation with small-molecule phosphodonors proceeds through the same chemistry that the phosphotransfer reaction [2], we

Table 3. Autophosphorylation rate constants (k_{app}) determined by fluorescence spectroscopy for the wild type (REC-WT) and mutant (REC-H85A) receiver domains using different concentrations of acetyl phosphate (AcP)

[AcP] (mM)	k_{app} (10^{-4} seg^{-1})[a]	
	REC-WT	REC-H85A
10	4.050 ± 0.004	1.77 ± 0.02
20	16.5 ± 0.3	1.90 ± 0.14
40	45.8 ± 4.1	3.18 ± 0.38

[a] Average rate constant ± SD.

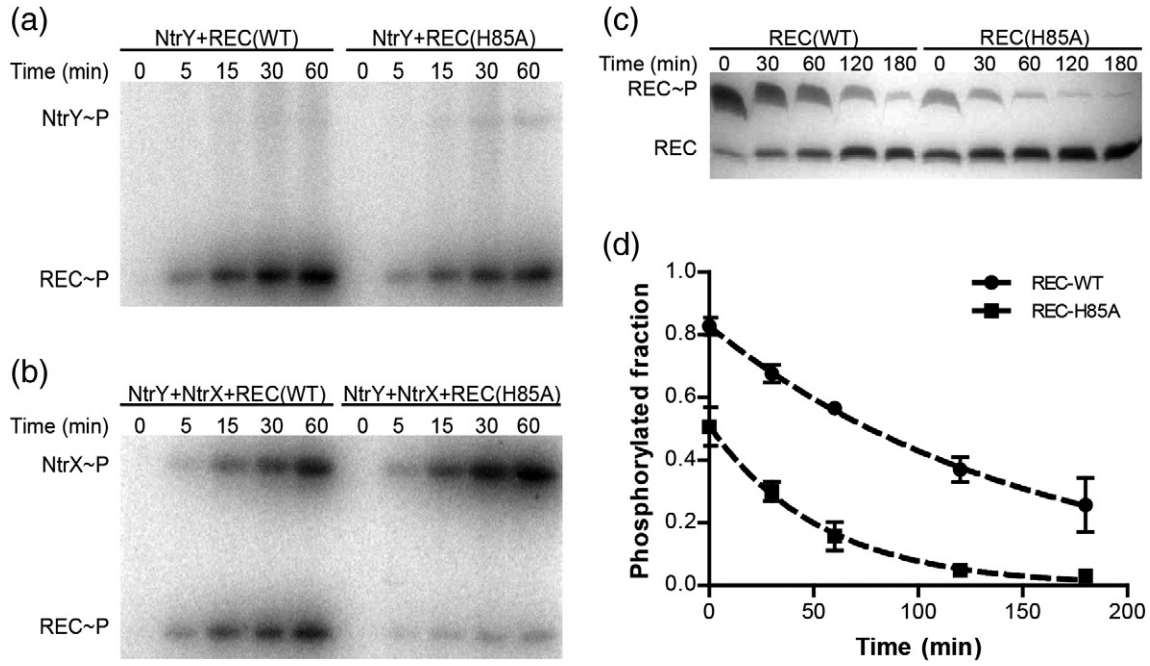

Fig. 5. Biochemical characterization of the NtrX REC domain and the effect of the H85A mutation. (a) A representative experiment of a phosphotransfer assay is shown. NtrY (PAS-HK construct) was incubated simultaneously with the NtrX REC domain (wild type or REC-H85A) and [γ-^{32}P]ATP. Aliquots were taken at different times and subjected to SDS-PAGE. The bands corresponding to radioactive REC domain or residual autophosphorylated NtrY are indicated. (b) Representative phosphotransfer experiment performed as described previously, but adding an equimolar amount of full-length NtrX. The bands corresponding to radioactive REC domain or NtrX are indicated (c) Phosphoprotein affinity gel electrophoresis was used to assess the autodephosphorylation activity of the wild type and H85A mutant REC domains. Each protein was phosphorylated with AcP and then the excess of phosphodonor was removed using a desalting column. Then, Mg^{2+} was added and aliquots were removed at different times and subjected to SDS-PAGE in gels prepared with Phos-tag™. In the representative experiment shown, the upper band corresponds to the phosphorylated domain. (d) From the phosphoprotein affinity gels, the phosphorylated fraction (intensity of the phosphorylated band with respect to the total intensity in the same lane) was obtained and the average of three independent experiments was plotted against time. The best-fit single decay function was fitted to obtain the dephosphorylation rate constant.

aimed to determine whether H85 could be important for the efficiency of phosphoryl transfer using the NtrY phosphohistidine as a substrate. We performed phosphotransfer experiments from phosphorylated NtrY [11] to either REC-WT or REC-H85A and found that the mutant domain is phosphorylated to a lesser extent than the wild type (Fig. 5a). Despite the fact that this result was obtained in several independent experiments, the differences were subtle in comparison with the severe impairment in autophosphorylation with AcP. In consequence, we decided to perform further experiments adding a molar equivalent of full-length NtrX, which has a wild-type receiver domain to compete for the phosphohistidine substrate. As expected, in the competition experiment, approximately 50% of the radioactive phosphate was detected in NtrX and the other 50% was detected in REC-WT (Fig. 5b). However, when the assay was performed using REC-H85A, there was a marked preference toward NtrX, with approximately 80% of the label incorporated to the full-length protein (Fig. 5b). This indicates that H85 is involved in the phosphotransfer reaction and that mutation of this residue affects the ability of the REC domain to phosphorylate using the phosphohistidine as a substrate, generating a kinetic disadvantage during the competition experiments.

We also established the autodephosphorylation rate constant of wild type and mutated REC-P domains. Figure 5c shows a representative experiment in which it is evident that the amount of phosphorylated REC-H85A is considerably lower at the beginning of the experiment (time 0) compared to REC-WT, confirming the phosphorylation defect in the mutant protein. Dephosphorylation rate constants were obtained from plots of phosphorylated fraction against time (Fig. 5d) and confirmed that the REC-WT domain dephosphorylates significantly more slowly (k_{deph} = 0.006 min^{-1}) than the REC-H85A mutant (k_{deph} = 0.018 min^{-1}). The rate constant value for NtrX REC domain is comparable to those of FixJ [35] and DctD [23] (0.005 and 0.007 min^{-1},

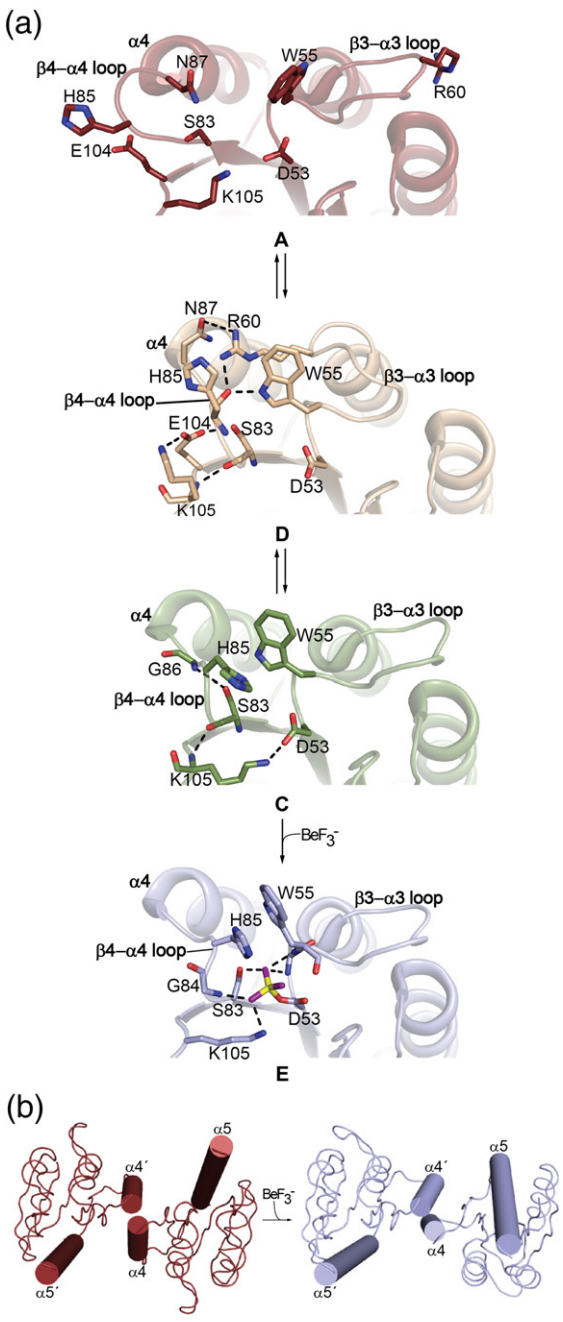

Fig. 6. Proposed model for activation and signal transduction. (a) Cartoon representation of the REC domain under different conformations, ordered according to the proposed conformational pathway that might explain the activation. Important residues for each structure are shown in sticks and the interactions between them are indicated with broken lines. The capital letter under the cartoon denotes the molecule designation used along this article. (b) Superposition of the dimeric structure of the inactive (red, left) and active (light blue, right) states of the REC domain that were modeled including their extended α5 helix. Phosphorylation reorients the α4 helix, leading to a rearrangement of the interface and a reorientation of the α5 helices.

respectively), both of which have a histidine residue at position 85.

To determine whether H85 influences the oligomeric state of the NtrX REC domain, we performed SEC-SLS experiments. The elution profile of REC-H85A (Fig. S5a) indicates that, in the inactive state, the protein is in monomer–dimer equilibrium, with estimated MMs close to those of REC-WT (Table 2). This indicates that the substitution of the histidine residue does not influence significantly the quaternary structure in the inactive state. When REC-H85A was phosphorylated with AcP, the domain eluted in two peaks (Fig. S5b) that were not completely resolved. As the concentration of the mutant domain increased, the MM corresponding to the first peak agreed better with that expected for a dimer (Table 2) and the second peak eluted in a lower volume with higher estimated MM. These results are consistent with partial phosphorylation of REC-H85A and indicate that, despite the mutation, REC-H85A is still able to dimerize.

Discussion

The prevailing conceptual framework for receiver domain activation has been that the protein exists in a dynamic equilibrium that accesses both an inactive and an active conformation [36]. Both states are populated in unphosphorylated REC domains, and phosphorylation shifts the equilibrium toward the active species. However, several crystal structures of the CheY RR show intermediate configurations [29,37,38] and recent NMR data supported a model of segmental motions underlying the activation of CheY, instead of a preexisting, concerted, two-state switch [39]. In the middle of this conceptual landscape, the structures of the isolated NtrX receiver domain argue against a simple equilibrium between inactive and active conformations since it was possible to crystallize "meta-active" conformations in the absence of the phosphorylation-mimic BeF_3^-. Even more, among those active-like species, different positions in the β3-α3 loop were observed, accounting for conformational diversity in the native state. Therefore, our results support that phosphorylation stabilizes a preexisting fraction of the REC domain population that samples the active conformation (rather than a phosphorylation-induced conformational change) that was achieved through segmental motions of different residues.

The crystallographic structures presented in this work allow us to postulate a possible conformational pathway to comprehend the allosteric changes of NtrX REC domain in which the β3-α3 loop plays a central role (Fig. 6a). Most of the RRs have a proline residue that generates a kink at this loop. However, that position is occupied by a glutamine (Q57) in

NtrX and the loop is extended by two amino acids (S59 and R60). NMR studies on NtrC REC domain [40] and molecular dynamics simulations on CheY have suggested that the β3-α3 loop is flexible [41], and in fact, two conformations were found in our REC-N structures. The conformational pathway that we propose starts from a ground state with both loops β3-α3 and β4-α4 opened (inactive state, molecules A and B from REC-N). Fluctuations in the β3-α3 loop position would lead to a closed state in which R60 is able to interact with backbone atoms from the β4-α4 loop (N87 and H85), stabilizing the closed conformation of both loops (molecule D from REC-N). This conformation also presents the β5-α5 loop in an altered position with K105 pointing away of the protein core and interacting with the E104 side chain, providing space for the displacement of the β4-α4 loop. Also, E104 interacts with S83, stabilizing the inward orientation of this key residue, which must flip in order to achieve an active state. Therefore, the molecule D from REC-N might represent an intermediary conformation where the closed state of loop β3-α3 contributes to an initial closure of the β4-α4 loop, which is also allowed by the movement of the loop β5-α5. Subsequently, the loop β4-α4 adopts an even more closed position and its conformation might be maintained by the interaction between W55 and H85, allowing the loop β3-α3 to return to an opened conformation (molecule C from REC-N) sustained by the interaction between R60 and D36 (from α2). In this state, K105 adopts a buried location and interacts with D53. Finally, the binding of beryllofluoride stabilizes this conformation through the interaction of the ligand with S83 and K105 and the parallel π stacking between W55 and H85. The proposed sequence of conformational transitions is supported by the fact that, among the meta-active structures reported, molecule C is the one that best resembles the active state, leaving conformation D as an intermediate state. Also, a previous article postulated that nonnative interactions are used to "hold on" to the free energy until the final new native contacts of the active state are built [42] and the analyzed interactions (Fig. 6a) might account for this role.

Even though the same secondary structure elements are involved in REC-N and REC-A dimer interfaces, the binding of beryllofluoride favors the displacement of the α4 helix to a position closer to the β5 strand from the opposite monomer. Also, an activated interface is created by opening a hydrophobic pocket at the N-terminal end of helix α4 and strand β5 with a specific T-G-X-G-X-Hyd-X3-Hyd-X2-Hyd motif that is frequently present in this assembly (Hyd: I88, V92, I95 in NtrX) [24]. Those changes lead to a more extensive interface (the buried surface area increases from 431 $Å^2$ in REC-N to 600 $Å^2$ in REC-A) that stabilizes the dimeric form of the receiver domain, as confirmed by the SEC-SLS experiments. Preliminary experiments indicate that nonphosphorylated full-length NtrX is a stable dimer in solution; therefore, the dimerization of the REC domain does not provide a mechanism for transmitting the phosphorylation signal to the rest of the NtrX molecule. The fact that the receiver domain is in monomer–dimer equilibrium in the native state might indicate that the dimerization of full-length NtrX depends on interactions between the remaining domains. A similar behavior was observed in NtrC4 from *Aquifex aeolicus*, which is a dimer in solution but its isolated REC domain is a monomer [43] as a consequence of using truncated domains rather than the full-length protein.

Superposition of dimeric structures from REC-N and REC-A indicates that the relative orientations of the α5 helices change drastically upon activation (Fig. 3b). Members of the NtrC subfamily of RRs usually have an extended α5 helix and NtrX is not an exception since secondary structure predictions indicate that this helix holds approximately 26 residues (in contrast to that of FixJ that has 15 amino acids). To gain insight into the changes that could take place in the full-length α5 helix, we traced the potential projection of this helix by molecular modeling of the dimeric structures of REC-N and REC-A (Fig. 6b). In this model, it is possible to observe that those helices from opposite monomers do not interact (then, they cannot form a coiled coil) and the superposition also indicates that, in REC-N, those helical segments are pointed away, whereas they point to a similar direction in the active form. Therefore, the projection of the α5 helices allows us to postulate that the changes in the active-state dimer interface would lead to a relative reorientation of these helices, which might contribute to the signal transduction toward the neighboring AAA+ domain. A previous article [43] analyzed the sequences of linker regions of NtrC-like RRs whose REC domains, as NtrX, contain the GHG motif. The authors found that 12% have a predicted coiled coil (like NtrC1 and DctD), 22% have a predicted unstructured linker (NtrC4), and the majority (65.5%) have variable amounts of helical structure but are not predicted to form a coiled coil. NtrX belongs to the latter group and the proposed reorientation of α5 helices as a transduction mechanism might be extended to a majority of proteins within this subfamily.

The activity of NtrC-like proteins is tightly regulated by either one of two postulated mechanisms [18]: (1) positive regulation, as seen in NtrC of enteric bacteria, in which phosphorylation of the receiver domain brings about a new interaction with the central domain, leading to the assembly of an active oligomer; (2) negative regulation, as seen in DctD and NtrC1, where the phosphorylation of the receiver domain leads to rearrangements that release the AAA+ domain so they can assemble an oligomer. A hint on the possible mechanism of regulation can be

obtained by studying the isolated receiver domain of a RR because it has been proved that the NtrC REC domain is a monomer in solution despite its phosphorylation status, whereas DctD and NtrC1 receiver domains are dimers in solution and phosphorylation selects an alternative dimeric state. We proved that the NtrX REC domain is under monomer–dimer equilibrium in solution and phosphorylation promotes dimerization, as has been reported for the HupR receiver domain [22]. HupR is another unusual RR among the NtrC-like family that lacks a functional GAFTGA motif, as does NtrX [20]. Therefore, this behavior of the isolated REC domains from NtrX and HupR in solution is neither consistent with the described positive regulation mechanism (NtrC) nor with the negative one (DctD or NtrC1) and may reflect an alternative activation mechanism valid for atypical members among the NtrC family that are not proper activators of σ^{54} promoters.

Our work provides, for the first time, insights into the activation mechanism of the NtrX RR. We conclude that phosphorylation selects preexisting dimeric states, which would lead to signal transduction from the REC domain to the rest of the molecule. Also, the different conformations observed in the crystals allowed us to postulate a pathway to comprehend the allosteric activation of RRs. Finally, by means of a mutant construct, we could identify H85 as an important residue for different catalytic activities performed by this REC domain. Even though further studies are required to evaluate possible changes in the oligomeric state of full-length NtrX and the relevance of different residues in the activation of the NtrY/X pathway *in vivo*, our work is an important contribution to understand the NtrY/X signaling system.

Materials and Methods

DNA manipulations

DNA manipulations were performed according to standard techniques. DNA encoding NtrX REC domain was amplified by PCR from the existing pET24a-NtrX construct [11] using the primers 5′-AAGGATC-CATGGCGGCCGATATTCTTGTTGT-3′ and 5′-TTCTCGAGCTTGAGCTTGGAGGTTTCCAGC-3′. The purified product was inserted into the pET24a vector (Novagen) using the restriction enzymes BamHI and XhoI. The final pET24a-REC(NtrX) construct, the quality of which was checked by DNA sequencing, includes the coding region of the REC domain (residues 1–126), 10 additional N-terminal residues (MASMTGGQQMGRGS) from the cloning procedure, 2 residues (LE) after the coding region, and a 6-residue-long C-terminal histidine tag.

The plasmid encoding the mutant protein REC-H85A was obtained from pET24a-REC(NtrX) by PCR amplification using the primers 5′-GTGATGATTTCCGGTGCTGGCAA-TATCGAAACCG-3′ and 5′-CGGTTTCGATATTGCCAG-CACCGGAAATCATCAC-3′, followed by digestion with the enzyme DpnI. All products are under control of the T7 promoter of the vector.

The plasmids encoding NtrY (soluble construct encompassing the PAS and HK domain, pET24d-PAS-HK-NtrY) and NtrX (full length, pET24a-NtrX) were prepared before [11].

Protein overexpression and purification

BL21(DE3)pLys cells were transformed with pET24a-REC or pET24a-REC-H85A and grown at 37 °C in 1 l of LB media with the appropriate antibiotic until absorbance (at 600 nm) reached 0.6. At this point, β-D-1-thiogalactopyranoside was added to a final concentration of 0.5 mM and the culture was incubated for another 16 h at 28 °C with agitation. The bacteria were centrifuged at 7000 rpm for 10 min at 4 °C. Pellets were resuspended in lysis buffer [20 mM Tris–HCl, 200 mM NaCl, 30 mM imidazole, and 1 mM phenylmethylsulfonyl fluoride (pH 8)], sonicated, and then centrifuged at 45,000 rpm in a Beckman Coulter L7-65 ultracentrifuge for 45 min at 4 °C. The supernatant was loaded into a HisTrap HP column (all columns were from GE Healthcare) in a high-performance liquid chromatography apparatus (GE Healthcare). Elution was performed with a linear gradient of buffer B [20 mM Tris–HCl, 200 mM NaCl, and 500 mM imidazole (pH 8)]. A major peak was observed at around 20% buffer B. The appropriate fractions were pooled and further purified by gel-filtration chromatography on a Superdex 75 column with isocratic elution in buffer I [20 mM Tris–HCl and 200 mM NaCl (pH 8)], yielding a major peak at around 70 ml. For fluorescence, light scattering, and activity experiments, a fraction of the total volume collected was directly concentrated by centrifugation in Amicon Ultra-4 devices (Millipore) and stored at −70 °C, while the rest was concentrated and simultaneously exchanged into crystallization buffer [10 mM Tris–HCl and 25 mM NaCl (pH 7.5)] and finally stored at −70 °C.

PAS-HK (NtrY) and NtrX were expressed and purified as reported previously [11].

Crystallization

Initial crystallization trials were made on 96-well plates using a Honeybee 963 robot (Digilab, Marlborough, MA, USA) and commercial crystallization kits from Jena Bioscience (Jena, Germany) and Hampton Research (Aliso Viejo, CA, USA). Optimized REC-N crystals were obtained by the hanging-drop method by mixing 2 μl of the concentrated protein stock with an equal amount of a crystallization solution consisting of 22% (w/v) polyethylene glycol (PEG) 550 monomethyl ether, 0.15 M malic acid, and 0.1 M imidazole (pH 7). Bar-shaped crystals with an approximate size of 0.1 mm × 0.1 mm × 0.3 mm appeared after 3 days of equilibration. For REC-A, freshly prepared 10× BeF_3^- solution (50 mM $BeCl_2$, 300 mM NaF, and 50 mM $MgCl_2$) was mixed with the protein solution in 1:10 proportion and then this sample was used for the crystallization trials. The best crystals grew within 3 days with the same method and volumes using 22% (w/v) PEG 400 and 0.1 M 4-morpholineethanesulfonic acid (pH 6.9) as precipitating agent, showing a significant smaller size (0.05 mm × 0.1 mm × 0.1 mm).

Samples were cryoprotected in their respective mother liquors added with PEG 400 and then cryocooled in liquid nitrogen.

X-ray data collection and processing

Native datasets were collected at 100 K on single crystals at the PROXIMA 1 protein crystallography beamline at the SOLEIL Synchrotron (France), which is equipped with a PILATUS 6M detector (Dectris, Baden, Switzerland). X-ray diffraction data were processed with XDS [44] running in a semiautomated mode using the xdsme package[†]. A total of 5% of the reflections were set aside for cross-validation. Detailed information on data collection parameters and processing statistics are presented in Table 1.

Structure resolution, model building, and refinement

The REC-N structure was solved by the molecular replacement method using the program Mr. Bump [45] from the CCP4 package [46]. The search model corresponded to the receiver domain of the *S. meliloti* DctD RR (PDB code 1L5Z [47]). The procedure included automatic trimming of the search probe with Sculptor [48], molecular replacement search with Phaser [49], and initial model building with Buccaneer [50]. A total of four copies of the molecule were successfully located in the asymmetric unit. Manual model building and refinement were performed with Coot [51] and BUSTER [52], respectively. REC-A was then solved by molecular replacement using REC-N as model, with two copies in the asymmetric unit. Detailed statistics on the refinement process and PDB deposition are found in Table 1.

Validation and analysis of the models

Both crystallographic models were validated with MolProbity [53]. The interface areas were obtained with PDBePISA [26] and the superpositions and RMSD calculations were performed with PDBeFold [54]. Sequence alignments were performed with ClustalW2 [55]. Figures were prepared using PyMOL (Schrödinger, New York, NY, USA).

Autophosphorylation with AcP followed by fluorescence spectroscopy

All fluorescence measurements were made using a Jasco FP-6500 spectrofluorimeter. Tryptophan fluorescence was measured at an excitation wavelength of 295 nm and an emission wavelength of 351 nm. Sample temperature was held at 25 °C by a circulating water bath.

Autophosphorylation reactions of REC-WT and REC-H85A were carried out in quartz cuvettes with manual mixing to initiate the reaction, and tryptophan fluorescence was continuously monitored. The beginning of the time traces was at 20 s after mixing. Different concentrations of REC domain (3, 5, 10, 20, and 30 μM) were prepared [20 mM Tris–HCl and 200 mM NaCl (pH 8)] and separately incubated with 50 mM AcP in order to establish protein concentration dependence and fluorescence recording began when 50 mM $MgCl_2$ was added to the cuvette. The REC domain was diluted [20 mM Tris–HCl and 200 mM NaCl (pH 8)] to a final concentration of 10 μM and incubated in different reactions with increasing amounts of the phosphodonor (5, 10, 20, 30, 40, 50, 60, and 80 μM for REC-WT; 10, 20, and 40 μM for REC-H85A) in order to determine the influence of AcP concentration and fluorescence recording began when 20 mM $MgCl_2$ was added to the cuvette. Reactions were performed in triplicate for each experimental condition.

Analysis of kinetic data

Autophosphorylation reactions were performed under pseudo-first-order conditions, with a large molar excess of AcP over protein, and were analyzed as reported elsewhere [32]. All time traces were normalized by dividing the fluorescence intensities by the initial fluorescence intensity to generate relative fluorescence intensity units (RFI). Initial curve fits were made to a single-exponential decay (GraphPad Prism). R^2 values of the fittings were greater than 0.9972 but systematic variations were observed during the first 150 s of reaction; thus, the rate constants derived were termed apparent rate constants (k_{app}). Plots of k_{app} *versus* the concentration of AcP for REC-WT appeared sigmoidal and were thus fit using a Hill equation (GraphPad Prism).

Static light scattering

The average molecular masses of REC-WT or REC-H85A were determined by SLS using a Precision detector PD2080 light-scattering instrument connected in tandem to a high-performance liquid chromatography system and an LKB 2142 differential refractometer. In each case, 500 μl of protein solution was injected into an analytical Superdex 75 column and eluted with a buffer consisting of 20 mM Tris–HCl and 200 mM NaCl (pH 8). The 90° light-scattering, absorbance at 280 nm and refractive index signals of the eluted protein were analyzed with the Discovery32 software supplied by Precision detectors. The 90° light-scattering detector was calibrated using bovine serum albumin (MM: 66.5 kDa) as a standard.

To achieve the *in vitro* phosphorylation of the samples, we prepared 500 μl of protein solution with 30 mM AcP and 30 mM $MgCl_2$, incubated it at 30 °C for 1 h, and then injected it into the Superdex 75 column.

Phosphoprotein affinity gel electrophoresis

Phos-tag™ acrylamide running gels contained 15% (w/v) 29:1 acrylamide/*N*′*N*′-methylenebisacrylamide, 375 mM Tris (pH 8.8), and 0.1% (w/v) SDS. Gels were copolymerized with 75 μM Phos-tag™ and 150 μM $ZnCl_2$. Stacking gels contained 4% (w/v) 29:1 acrylamide/*N*′*N*′-methylenebisacrylamide, 125 mM Tris (pH 6.8), and 0.1% (w/v) SDS. All Phos-tag™ acrylamide containing gels were run with standard denaturing running buffer at 4 °C under constant voltage (150 V). The fraction of phosphorylated protein in each gel lane was determined by quantifying the Coomassie Blue staining intensity (Quantity One,

BioRad) for the upshifted (phosphorylated) protein band in each lane relative to the total staining intensity for both bands (total protein) in the lane.

Receiver domain autodephosphorylation analysis

REC-WT and REC-H85A were separately phosphorylated as follows: 500-μl solutions of 100 μM protein were prepared in reaction buffer [20 mM Tris–HCl and 200 mM NaCl (pH 8)] containing 30 mM AcP and 30 mM $MgCl_2$. The reaction was allowed to proceed for 2 h at 30 °C and then the 500-μl solutions were loaded into a G25 desalting column (previously equilibrated in reaction buffer) to remove the excess of AcP and $MgCl_2$. Eluate (800 μl) was recovered, quantified, diluted to 20 μM, and then we added 20 mM $MgCl_2$ Aliquots (50 μl) were removed at different times (0, 30, 60, 120, and 180 min) and quenched by the addition of 10 μl of 6× SDS loading buffer. Quenched samples were kept on ice until the last time point was obtained, and finally, the extent of protein phosphorylation was determined using phosphoprotein affinity gel electrophoresis. The rate of autodephosphorylation was determined from fits of the phosphorylated fraction (an average of three independent experiments) *versus* time using a single-exponential decay function (GraphPad Prism).

Phosphotransfer from [^{32}P]NtrY-P to NtrX receiver domain

PAS-HK (NtrY) (10 μM) was reduced [11] and incubated with either 10 μM REC-WT or REC-H85A in reaction buffer [20 mM Tris–HCl, 200 mM NaCl, and 5 mM $MgCl_2$ (pH 8)]. The reaction was started by addition of 0.1 mM of ATP containing 0.5 μCi of [γ-^{32}P]ATP (3000 Ci/mmol; Perkin Elmer) at room temperature and 20-μl samples were removed and added to an equal volume of 2× SDS-PAGE buffer at the following time points: 0, 5, 15, 30, and 60 min. Samples were electrophoresed on 15% polyacrylamide gels. The gels were dried and exposed to a Store Phosphor Screen (GE Healthcare). The screen was scanned using a Storm Image and Detection system (Molecular Dynamics).

For competition assays, 10 μM PAS-HK was reduced and incubated simultaneously with 10 μM REC-WT (or REC-H85A) and 10 μM NtrX (full length) in reaction buffer. The rest of the protocol was followed as detailed previously. Finally, the intensity of the bands was quantified using Quantity One (BioRad) and the percentage of radioactive label corresponding to NtrX-P or REC-P was obtained as the intensity of the selected band relative to the total intensity in that lane.

Modeling of NtrX REC domain with full-length α5 helices

The NtrX REC domain sequence (residues 1–135) was introduced in the SWISS-MODEL server [56–58], and homology models were obtained using DctD REC domain in their inactive state (PDB code 1QKK) or bound to beryllofluoride (PDB code 1L5Y) as templates. The modeled structures were then aligned to each monomer in either REC-N (molecules A and B) or REC-A (molecules E and F), respectively, to generate the dimeric state.

Accession numbers

The coordinates of NtrX REC domain structures in the absence of ligand (REC-N) and bound to beryllofluoride and magnesium (REC-A) have been deposited in the PDB with accession codes 4D6X and 4D6Y, respectively.

Supplementary data to this article can be found online at http://dx.doi.org/10.1016/j.jmb.2015.06.010.

Acknowledgment

We thank Daniela Di Bella for her help with the preparation of figures. This work was supported by a grant from Agencia Nacional de Promoción Científica y Tecnológica (PICT-2013-1629). We also acknowledge access to the X-ray facilities at the SOLEIL synchrotron (France) and the Argentinian Ministry of Science, Technology, and Productive Innovation for travel support. L.H.O., S.K., M.C.C., and F.A.G. are researchers from CONICET. I.F. is a recipient of a fellowship from CONICET.

Received 9 March 2015;
Received in revised form 11 May 2015;
Accepted 17 June 2015
Available online 23 June 2015

Keywords:
Brucella abortus;
REC domain;
response regulator;
two-component system;
NtrY

†http://code.google.com/p/xdsme/.

Abbreviations used:
HK, histidine kinase; RR, response regulator; bEBP, bacterial enhancer binding protein; SEC, size-exclusion chromatography; SLS, static light scattering; MM, molecular mass; PEG, polyethylene glycol.

References

[1] A.M. Stock, V.L. Robinson, P.N. Goudreau, Two-component signal transduction, Annu Rev Biochem 69 (2000) 183–215.
[2] R. Gao, A.M. Stock, Biological insights from structures of two-component proteins, Annu Rev Microbiol 63 (2009) 133–154.
[3] G.S. Lukat, W.R. McCleary, A.M. Stock, J.B. Stock, Phosphorylation of bacterial response regulator proteins by low molecular weight phospho-donors, Proc Natl Acad Sci U S A 89 (1992) 718–722.
[4] R.E. Silversmith, J.L. Appleby, R.B. Bourret, Catalytic mechanism of phosphorylation and dephosphorylation of CheY: kinetic characterization of imidazole phosphates as

phosphodonors and the role of acid catalysis, Biochemistry 36 (1997) 14965–14974.
[5] S.S. Da Re, D. Deville-Bonne, T. Tolstykh, M. V. r., J.B. Stock, Kinetics of CheY phosphorylation by small molecule phosphodonors, FEBS Lett 457 (1999) 323–326.
[6] D. Yan, H.S. Cho, C.A. Hastings, M.M. Igo, S.Y. Lee, J.G. Pelton, et al., Beryllofluoride mimics phosphorylation of NtrC and other bacterial response regulators, Proc Natl Acad Sci U S A 96 (1999) 14789–14794.
[7] M.J. Corbel, Brucellosis: an overview, Emerg Infect Dis 3 (1997) 213–221.
[8] S. Kohler, V. Foulongne, S. Ouahrani-Bettache, G. Bourg, J. Teyssier, M. Ramuz, et al., The analysis of the intramacrophagic virulome of *Brucella suis* deciphers the environment encountered by the pathogen inside the macrophage host cell, Proc Natl Acad Sci U S A 99 (2002) 15711–15716.
[9] J. Ariza, C. Pigrau, C. Canas, A. Marron, F. Martinez, B. Almirante, et al., Current understanding and management of chronic hepatosplenic suppurative brucellosis, Clin Infect Dis 32 (2001) 1024–1033.
[10] D. Colmenero Jde, M.I. Queipo-Ortuno, J. Maria Reguera, M. Angel Suarez-Munoz, S. Martin-Carballino, P. Morata, Chronic hepatosplenic abscesses in Brucellosis. Clinico-therapeutic features and molecular diagnostic approach, Diagn Microbiol Infect Dis 42 (2002) 159–167.
[11] C. Carrica Mdel, I. Fernandez, M.A. Marti, G. Paris, F.A. Goldbaum, The NtrY/X two-component system of *Brucella* spp. acts as a redox sensor and regulates the expression of nitrogen respiration enzymes, Mol Microbiol 85 (2012) 39–50.
[12] C. Carrica Mdel, I. Fernandez, R. Sieira, G. Paris, F.A. Goldbaum, The two-component systems PrrBA and NtrYX co-ordinately regulate the adaptation of *Brucella abortus* to an oxygen-limited environment, Mol Microbiol 88 (2013) 222–233.
[13] K. Pawlowski, U. Klosse, F.J. de Bruijn, Characterization of a novel *Azorhizobium caulinodans* ORS571 two-component regulatory system, NtrY/NtrX, involved in nitrogen fixation and metabolism, Mol Gen Genet 231 (1991) 124–138.
[14] Y. Kumagai, Z. Cheng, M. Lin, Y. Rikihisa, Biochemical activities of three pairs of *Ehrlichia chaffeensis* two-component regulatory system proteins involved in inhibition of lysosomal fusion, Infect Immun 74 (2006) 5014–5022.
[15] J.M. Atack, Y.N. Srikhanta, K.Y. Djoko, J.P. Welch, N.H. Hasri, C.T. Steichen, et al., Characterization of an *ntrX* mutant of *Neisseria gonorrhoeae* reveals a response regulator that controls expression of respiratory enzymes in oxidase-positive proteobacteria, J Bacteriol 195 (2013) 2632–2641.
[16] D. Wang, H. Xue, Y. Wang, R. Yin, F. Xie, L. Luo, The *Sinorhizobium meliloti ntrX* gene is involved in succinoglycan production, motility, and symbiotic nodulation on alfalfa, Appl Environ Microbiol 79 (2013) 7150–7159.
[17] J.M. Skerker, M.S. Prasol, B.S. Perchuk, E.G. Biondi, M.T. Laub, Two-component signal transduction pathways regulating growth and cell cycle progression in a bacterium: a system-level analysis, PLoS Biol 3 (2005) e334.
[18] M. Bush, R. Dixon, The role of bacterial enhancer binding proteins as specialized activators of sigma54-dependent transcription, Microbiol Mol Biol Rev 76 (2012) 497–529.
[19] W.C. Bowman, R.G. Kranz, A bacterial ATP-dependent, enhancer binding protein that activates the housekeeping RNA polymerase, Genes Dev 12 (1998) 1884–1893.
[20] W. Dischert, P.M. Vignais, A. Colbeau, The synthesis of *Rhodobacter capsulatus* HupSL hydrogenase is regulated by the two-component HupT/HupR system, Mol Microbiol 34 (1999) 995–1006.
[21] Z. Cheng, M. Lin, Y. Rikihisa, *Ehrlichia chaffeensis* proliferation begins with NtrY/NtrX and PutA/GlnA upregulation and CtrA degradation induced by proline and glutamine uptake, MBio 5 (2014) e02141.
[22] K.M. Davies, E.D. Lowe, C. Venien-Bryan, L.N. Johnson, The HupR receiver domain crystal structure in its nonphospho and inhibitory phospho states, J Mol Biol 385 (2009) 51–64.
[23] M.G. Meyer, S. Park, L. Zeringue, M. Staley, M. McKinstry, R.I. Kaufman, et al., A dimeric two-component receiver domain inhibits the sigma54-dependent ATPase in DctD, FASEB J 15 (2001) 1326–1328.
[24] M. Doucleff, B. Chen, A.E. Maris, D.E. Wemmer, E. Kondrashkina, B.T. Nixon, Negative regulation of AAA+ ATPase assembly by two component receiver domains: a transcription activation mechanism that is conserved in mesophilic and extremely hyperthermophilic bacteria, J Mol Biol 353 (2005) 242–255.
[25] R.B. Bourret, Receiver domain structure and function in response regulator proteins, Curr Opin Microbiol 13 (2010) 142–149.
[26] E. Krissinel, K. Henrick, Inference of macromolecular assemblies from crystalline state, J Mol Biol 372 (2007) 774–797.
[27] A. Toro-Roman, T.R. Mack, A.M. Stock, Structural analysis and solution studies of the activated regulatory domain of the response regulator ArcA: a symmetric dimer mediated by the alpha4-beta5-alpha5 face, J Mol Biol 349 (2005) 11–26.
[28] P. Bachhawat, G.V. Swapna, G.T. Montelione, A.M. Stock, Mechanism of activation for transcription factor PhoB suggested by different modes of dimerization in the inactive and active states, Structure 13 (2005) 1353–1363.
[29] M. Simonovic, K. Volz, A distinct meta-active conformation in the 1.1-Å resolution structure of wild-type ApoCheY, J Biol Chem 276 (2001) 28637–28640.
[30] F. Trajtenberg, D. Albanesi, N. Ruetalo, H. Botti, A.E. Mechaly, M. Nieves, et al., Allosteric activation of bacterial response regulators: the role of the cognate histidine kinase beyond phosphorylation, MBio 5 (2014) e02105.
[31] B.E. Scharf, Summary of useful methods for two-component system research, Curr Opin Microbiol 13 (2010) 246–252.
[32] R.L. Creager-Allen, R.E. Silversmith, R.B. Bourret, A link between dimerization and autophosphorylation of the response regulator PhoB, J Biol Chem 288 (2013) 21755–21769.
[33] S.A. Thomas, R.M. Immormino, R.B. Bourret, R.E. Silversmith, Nonconserved active site residues modulate CheY autophosphorylation kinetics and phosphodonor preference, Biochemistry 52 (2013) 2262–2273.
[34] S.A. Thomas, J.A. Brewster, R.B. Bourret, Two variable active site residues modulate response regulator phosphoryl group stability, Mol Microbiol 69 (2008) 453–465.
[35] M. Weinstein, A.F. Lois, G.S. Ditta, D.R. Helinski, Mutants of the two-component regulatory protein FixJ of *Rhizobium meliloti* that have increased activity at the *nifA* promoter, Gene 134 (1993) 145–152.
[36] B.F. Volkman, D. Lipson, D.E. Wemmer, D. Kern, Two-state allosteric behavior in a single-domain signaling protein, Science 291 (2001) 2429–2433.
[37] C.M. Dyer, F.W. Dahlquist, Switched or not?: the structure of unphosphorylated CheY bound to the N terminus of FliM, J Bacteriol 188 (2006) 7354–7363.
[38] J. Guhaniyogi, V.L. Robinson, A.M. Stock, Crystal structures of beryllium fluoride-free and beryllium fluoride-bound CheY in complex with the conserved C-terminal peptide of CheZ reveal dual binding modes specific to CheY conformation, J Mol Biol 359 (2006) 624–645.

[39] L.R. McDonald, J.A. Boyer, A.L. Lee, Segmental motions, not a two-state concerted switch, underlie allostery in CheY, Structure 20 (2012) 1363–1373.
[40] C.A. Hastings, S.Y. Lee, H.S. Cho, D. Yan, S. Kustu, D.E. Wemmer, High-resolution solution structure of the beryllofluoride-activated NtrC receiver domain, Biochemistry 42 (2003) 9081–9090.
[41] M.H. Knaggs, F.R. Salsbury, M.H. Edgell, J.S. Fetrow, Insights into correlated motions and long-range interactions in CheY derived from molecular dynamics simulations, Biophys J 92 (2007) 2062–2079.
[42] A.K. Gardino, J. Villali, A. Kivenson, M. Lei, C.F. Liu, P. Steindel, et al., Transient non-native hydrogen bonds promote activation of a signaling protein, Cell 139 (2009) 1109–1118.
[43] J.D. Batchelor, M. Doucleff, C.J. Lee, K. Matsubara, S. De Carlo, J. Heideker, et al., Structure and regulatory mechanism of *Aquifex aeolicus* NtrC4: variability and evolution in bacterial transcriptional regulation, J Mol Biol 384 (2008) 1058–1075.
[44] W. Kabsch, Xds, Acta Crystallogr D Biol Crystallogr 66 (2010) 125–132.
[45] R.M. Keegan, M.D. Winn, Automated search-model discovery and preparation for structure solution by molecular replacement, Acta Crystallogr D Biol Crystallogr 63 (2007) 447–457.
[46] M.D. Winn, C.C. Ballard, K.D. Cowtan, E.J. Dodson, P. Emsley, P.R. Evans, et al., Overview of the CCP4 suite and current developments, Acta Crystallogr D Biol Crystallogr 67 (2011) 235–242.
[47] S. Park, M. Meyer, A.D. Jones, H.P. Yennawar, N.H. Yennawar, B.T. Nixon, Two-component signaling in the AAA+ ATPase DctD: binding Mg^{2+} and BeF3- selects between alternate dimeric states of the receiver domain, FASEB J 16 (2002) 1964–1966.
[48] G. Bunkoczi, R.J. Read, Improvement of molecular-replacement models with Sculptor, Acta Crystallogr D Biol Crystallogr 67 (2011) 303–312.
[49] A.J. McCoy, R.W. Grosse-Kunstleve, P.D. Adams, M.D. Winn, L.C. Storoni, R.J. Read, Phaser crystallographic software, J Appl Crystallogr 40 (2007) 658–674.
[50] K. Cowtan, The Buccaneer software for automated model building. 1. Tracing protein chains, Acta Crystallogr D Biol Crystallogr 62 (2006) 1002–1011.
[51] P. Emsley, B. Lohkamp, W.G. Scott, K. Cowtan, Features and development of Coot, Acta Crystallogr D Biol Crystallogr 66 (2010) 486–501.
[52] G. Bricogne, E. Blanc, M. Brandl, C. Flensburg, P. Keller, W. Paciorek, P. Roversi, A. Sharff, O.S. Smart, C. Vonrhein, T.O. Womack, BUSTER version 2.10.1, Global Phasing Ltd, Cambridege, United Kingdom, 2014.
[53] V.B. Chen, W.B. Arendall, J.J. Headd, D.A. Keedy, R.M. Immormino, G.J. Kapral, et al., MolProbity: all-atom structure validation for macromolecular crystallography, Acta Crystallogr D Biol Crystallogr 66 (2010) 12–21.
[54] E. Krissinel, K. Henrick, Secondary-structure matching (SSM), a new tool for fast protein structure alignment in three dimensions, Acta Crystallogr D Biol Crystallogr 60 (2004) 2256–2268.
[55] M.A. Larkin, G. Blackshields, N.P. Brown, R. Chenna, P.A. McGettigan, H. McWilliam, et al., Clustal W and Clustal X version 2.0, Bioinformatics 23 (2007) 2947–2948.
[56] K. Arnold, L. Bordoli, J. Kopp, T. Schwede, The SWISS-MODEL workspace: a Web-based environment for protein structure homology modelling, Bioinformatics 22 (2006) 195–201.
[57] M. Biasini, S. Bienert, A. Waterhouse, K. Arnold, G. Studer, T. Schmidt, et al., SWISS-MODEL: modelling protein tertiary and quaternary structure using evolutionary information, Nucleic Acids Res 42 (2014) W252–W258.
[58] F. Kiefer, K. Arnold, M. Kunzli, L. Bordoli, T. Schwede, The SWISS-MODEL repository and associated resources, Nucleic Acids Res 37 (2009) D387–D392.